Hindawi
Mathematical Problems in Engineering
Volume 2022, Article ID 6749649, 14 pages
https://doi.org/10.1155/2022/6749649

Research Article

Integrated Direct Yaw Control and Antislip Regulation Mixed Control of Distributed Drive Electric Vehicle Using Cosimulation Methodology

Xinwen Zhang,[1] **Hongbo Liang**,[2] **Xiehui Wang**,[3] **and Qiang Li**[1]

[1]*Zhejiang University of Science and Technology, Hangzhou 310023, China*
[2]*Anhui Communications Vocational & Technical College, Hefei 340100, China*
[3]*ZF Transmission Technology (Jiaxing) Co., Ltd., Jiaxing 314000, China*

Correspondence should be addressed to Hongbo Liang; 472657312@qq.com

Received 11 February 2022; Accepted 22 October 2022; Published 9 December 2022

Academic Editor: A. M. Bastos Pereira

The improvement of handling and stability performance of Distributed Drive Electric Vehicle (DDEV) is analyzed, visualized, and designed by proposing and deploying the mixed control strategies in this paper including Direct Yaw Control (DYC), Antislip Regulation (ASR) and a novel Dual-mode Switching Control (DMSC). First, by drawing the phase trajectory stability domain, the vehicle stability limit boundary can be determined, which provides the basis for the lateral stability constraint of the vehicle. Then, the practicability and real time visualization of driving efficiency and timeliness of DDEV is achieved to reduce the margin of error for the desired torque value by employing the DYC strategy which uses a fuzzy PID algorithm. Furthermore, the ASR strategy which adopts the optimal slip rate algorithm to determine the requirement of desired torque value based on the different road conditions is used to reduce slip phenomenon effectively and to maintain handling control of DDEV. In response to different scenes especially conflict and coexistence between DYC and ASR, the DMSC strategy is applied to find a more suitable slip rate range by using the root mean square error method (REME). Finally, the cosimulation platform of ADAMS/Car and MATLAB/Simulink is built to simulate the mixed control strategies by integrating DYC, ASR, and DMSC. The simulation results show that the DMSC can effectively prevent DDEV from entering the dangerous limit driving state when turning and driving. The strategy has a more significant control effect needed to meet the requirements of the driving safety of the vehicle and handling stability. The DMSC is adopted and downloaded into the electronic control unit of our student type formula vehicle called Flash V6 which was designed and developed by a team of students, the ZUST ATTACKER Team.

1. Introduction

Distributed drive electric vehicle (DDEV) is an important development and design direction of future electric vehicles. Their main features are that the drive motor is embedded in the wheel, the transmission chain is shorter, the speed response is faster and the torque control accuracy is high [1]. The wheels equipped with the drive motors can not only be independently controlled but also the wheel torque can be arbitrarily distributed to achieve optimum and better control effect. Based on these characteristics, a torque optimization control algorithm was designed [2] and combined with the quadratic programming method to design a torque average distribution algorithm [3]. Junjun et al. [4] proposed a particle swarm optimization and nonlinear predictive control algorithm through torque optimization and distribution to improve the vehicle stability while Jingxing et al. [5] used the expected additional torque obtained by a linear quadratic regulator (LQR). The more common schemes in torque control include uses the yaw rate as the feedback object which is obtained by the optimal allocation strategy [6] and combined with the slip rate normally used to construct ABS which prevents vehicle instability [7]. The yaw rate and the side slip angle are not only used as parameters to observe the vehicle response [8, 9] but also combined with the sliding mode controller. These strategies

based on multiple sliding mode controls [10–12] were used to design a torque distribution system needed for torque redistribution while ensuring the stability of vehicle braking.

Meanwhile, the slip rate can also be used as a reference value to study the ASR strategy. Based on the independent driving electric vehicles models, the conventional method of slip rate calculations were used to improve the vehicle longitudinal driving stability [13]. Through the fuzzy PID controller, the motor torque is adjusted to obtain the best slip rate control [14–16] which shortens the driving acceleration distance and improves the steering stability [17]. Based on fuzzy PID control theory [18], the integrated control strategy of ASR and DYC with a feed forward-feedback method were designed as the active front wheel steering controller (AFS) and DYC which are used as new controllers to obtain a target drive torque that could effectively improve vehicle stability [19]. The dynamic DYC combined with feed forward and feedback control system was proposed to improve the stability of the vehicle [20]. A layered control strategy is designed for distributed drive electric vehicles [21], taking the longitudinal stability of the vehicle as the goal, considering the lateral and longitudinal force coupling of the tires and layered control of the motor and hydraulic brake composite distribution control is designed, which is verified by the joint simulation of Carsim and MATLAB/Simulink, which can effectively improve the vehicle stability. Pacejka [22] used the front axle slip angle-rear axle slip angle phase plane to analyze the influence of tire nonlinear dynamic characteristics on vehicle handling stability.

Based on the above-given excellent research works, the phase trajectory stability domain and DYC/ASR controller were introduced in DMSC to achieve the purpose of correcting the driving state of the vehicle, the multimode control strategy was designed to improve the longitudinal/lateral stability of the vehicle, which is integrated into the DMSC of DYC algorithm with fuzzy PID controller and ASR algorithm with optimal slip rate PID controller. Finally, establishing the cosimulation platform using ADAMS®/Car and MATLAB®/Simulink, and the effectiveness and practicability of the control strategies were finally verified using a real DDEV.

2. Modeling of the DDEV

2.1. Vehicle Dynamic Model. In order to improve the operating efficiency of the control model and better reflect the vehicle kinematics and dynamic characteristics, the two degrees of freedom (2-DOF) linear vehicle model [23] is used as the following reference model:

$$\begin{cases} K_1\left(\beta_d + \dfrac{a\gamma_d}{v} - \delta_f\right) + K_2\left(\beta_d - \dfrac{b\gamma_d}{v}\right) = m\left(\dot{v}_y + u\gamma_d\right), \\ \mathrm{aK}_1\left(\beta_d + \dfrac{a\gamma_d}{v} - \delta_f\right) + bK_2\left(\beta_d - \dfrac{b\gamma_d}{v}\right) = I_z\dot{\gamma}_d. \end{cases} \tag{1}$$

According to the transformation formula:

$$\begin{cases} \dot{\gamma}_d = \dfrac{a^2K_1 + b^2K_2}{I_z v}\gamma_d + \dfrac{aK_1 - bK_2}{I_z} - \dfrac{aK_1}{I_z}\delta_f, \\ \dot{\beta}_d = \left(\dfrac{aK_1 - bK_2}{mv^2} - 1\right)\gamma_d + \dfrac{K_1 + K_2}{\mathrm{mv}}\gamma_d - \dfrac{K_1}{\mathrm{mv}}\delta_f, \end{cases} \tag{2}$$

where v is the longitudinal speed; v_y is the velocity of the center of mass; δ_f is the front wheel angle.

According to formula (2), δ_f with v are used as input variables; the desired yaw rate γ_d and side slip angle β_d are obtained by establishing 2-DOF linear vehicle model in Simulink.

2.2. Electric Power Flow Model. Emrax 188 motor is used in the DDEV, because of the reliability of permanent magnet synchronous motors. Their mechanical characteristics include simple structure, small volume, less cumbersome, rapid response, high power density, and efficiency. According to the relevant parameters in Table 1, a simplified motor model is established as the torque demand command actuator in the vehicle control strategy. By adjusting the current in the motor model, the motor can output smooth torque to the driving wheel.

In order to make the motor torque command response as close to the real motor characteristics as possible, the motor driver is regarded as the first-order inertial link when building the simplified model of the motor as shown in the following formula:

$$T_w = \frac{1}{1 + \tau s} \times T_m, \tag{3}$$

where T_w is the actual torque of the motor, τ is the time constant obtained from the motor characteristic parameters, T_m is the external characteristic torque of the motor.

In order to describe the characteristics of the motor, the transfer function equation of the motor is established and combined with the motor parameters. The model diagram is shown in Figure 1.

Here, T_{dl} is target torque of left wheel, T_{dr} represents right wheel target torque, e_T is the torque difference, U_x is the motor terminal voltage value, e_U is the voltage difference, I is the armature current, K_e is the electromagnetic torque constant, K_w is the induced electromotive force constant, U_w is the induced electromotive force value, T_{ml} is the left wheel motor output torque, T_{mr} is the right wheel motor output torque, w_{rr} actual angular velocity of right wheel, w_{rl} actual angular velocity of left wheel, T_{rl} is the actual torque of left wheel, T_{rr} is the actual torque of right wheel.

2.3. Establishment of Vehicle Model

2.3.1. Vehicle Framework. The electric vehicle model with distributed driven wheels was constructed using ADAMS/Car software while the motor model and control strategy with the MATLAB/Simulink software. Setting the relevant parameters at the communication interface between ADAMS/Car and MATLAB/Simulink, the real-time data interaction channel of

Table 1: Related parameters of EMRAX 188 motor.

Symbol	Parameters	Value and units
P_t	Peak power	65 kW
P_c	Continuous power	35 kW
T_t	Peak torque	90 N·m
T_c	Continuous torque	50 N·m
n_e	Rated speed	7000 rpm
n_t	Max. speed	8500 rpm

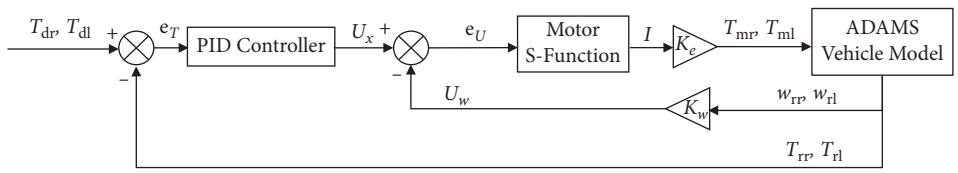

Figure 1: Motor model diagram.

ADAMS/Car and MATLAB/Simulink was established, and the two parts of the model were jointly simulated. The overall architecture is illustrated as shown in Figure 2.

2.3.2. Vehicle Parameters. The vehicle model established in ADAMS/Car software according to the parameters in Table 2 are referenced with our student type formula vehicle called Flash V6. And, the vehicle model built by ADMAS/Car is shown in Figure 3.

3. Control Strategy Design

3.1. Defining Stable Regions. The phase plane method is a common method for analyzing vehicle stability. By drawing the phase trajectory stability domain, the vehicle stability limit boundary can be determined. Many scholars use the centroid sideslip angle-centroid sideslip angle velocity phase plane method to analyze the vehicle driving stability [24, 25]. In order to analyze the stable area of the vehicle, the differential equation of the derivative and the derivative is established according to the 2-DOF model, and the tire force is calculated from the tire model under pure slip conditions. Combined with different settings and initial values, different vehicle speeds are obtained. The stable area under the adhesion coefficient with the road surface, the simulation flow chart is shown in Figure 4.

Separately, the phase plane method set two cases. Under case 1, high adhesion coefficient and different speeds, and case 2, high speed and different adhesion coefficient. After the corresponding phase trajectories are generated, respectively, the change rule is summarized in Tables 3 and 4.Here, $|X|$ is the absolute value of the coordinates of the rhombus stable boundary with γ, $|Y|$ is the absolute value of the coordinates of the rhombus stable boundary with β, μ is the adhesion coefficient.

3.2. DYC Module. The DYC module is mainly used to calculate the additional yaw torque produced by the vehicle around the center of mass when turning, adjust the yaw motion state of the vehicle, and then participate in the driving torque distribution module of the vehicle.

Based on the 2-DOF linear vehicle model, the ideal state of the vehicle is obtained as γ_d and β_d. By tracking these two variables which reflect the actual state of the vehicle and how it can quickly become stable thus the actual value can continuously tend to the expected value. By making a difference, we can get $e_1 = \gamma - \gamma_d$ and $e_2 = \beta - \beta_d$ input fuzzy PID controller to get ΔM_1 as shown in Figure 5.

Defined variable:

$$S = \xi_1 \times (\gamma\text{-}\gamma_{\mathrm{d}}) + \xi_2 \times (\beta\text{-}\beta_{\mathrm{d}}), \tag{4}$$

where ξ_1 and ξ_2 are the weight coefficients, which are obtained by the established fuzzy rule controller in Table 5.

According to formula (4) and Table 5, the ΔM_1 is obtained:

$$\Delta M_1 = \mathrm{k}_1 \times \mathrm{fuzzy}(S), \tag{5}$$

where k_1 is the fuzzy function known as Mamdani fuzzy rule controller.

Neglecting the road interference in the process of vehicle driving, the ΔM_1 obtained needs to be converted to the torque value acting on the driving wheel and the following formula is used:

$$\Delta M_1 = \Delta F \times T_{\mathrm{r}} = (\Delta F_{\mathrm{l}}\text{-}\Delta F_{\mathrm{r}}) \times \frac{T_{\mathrm{r}}}{2}, \tag{6}$$

where ΔF is the corrected driving force.

It is noted that the relationship between driving torque and driving force of the wheel is given as follows:

$$\Delta T = \Delta F \times r = \frac{|\Delta M_1| \times \mathrm{r}}{T_{\mathrm{r}}}, \tag{7}$$

where r is the wheel rolling radius, and ΔT is the torque the motor need to adjust when maintaining the body posture under the current driving conditions.

The redistributed torque values are obtained by combining (6) and (7):

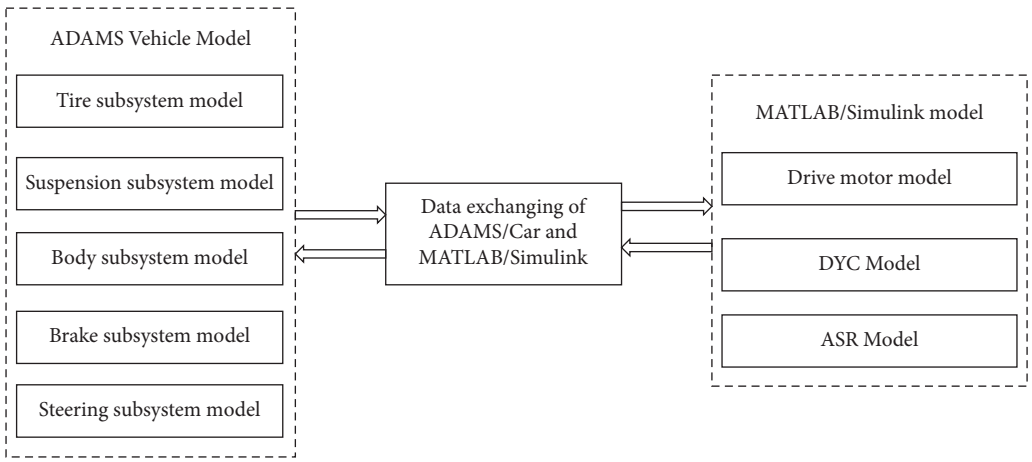

Figure 2: Schematic diagram of vehicle and control models architecture.

Table 2: Related parameters of vehicle model.

Symbol	Parameters	Value and units
m	Vehicle mass	320 kg
a	Distance from centroid to front axle	0.81 m
b	Distance from centroid to rear axle	0.89 m
T_f	Front tread	1.22 m
T_r	Rear tread	1.18 m
h	Height of center of gravity	0.24 m

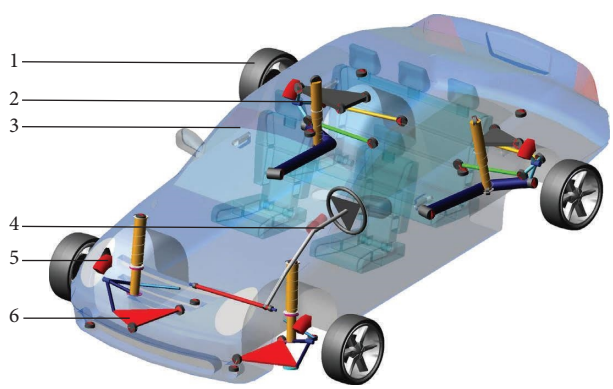

Figure 3: ADAMS/car vehicle model. 1-front and rear tire system 2-rear suspension system 3-body subsystem 4-steering subsystem 5-brake subsystem 6-front suspension system.

$$\begin{cases} T_{dl} = T_d, \quad T_{dr} = T_d \quad \Delta M_1 = 0 \\ T_{dl} = T_d - \Delta T/2, \quad T_{dr} = T_d + \Delta T/2 \quad \Delta M_1 > 0, \\ T_{dl} = T_d + \Delta T/2, \quad T_{dr} = T_d - \Delta T/2 \quad \Delta M_1 < 0 \end{cases} \tag{8}$$

where T_d is the product of the switch opening and the theoretical maximum output torque of the motor.

3.3. ASR Module. The purpose of the ASR module is to obtain the additional yaw torque value that needs to be applied to prevent the wheel from slipping during the driving process and use the road surface information to obtain the force required to control the normal steering of the vehicle to improve the vehicle handling stability and driving safety. The direct driving force of the vehicle comes from the friction reaction between the driving wheel and the ground and its limit value is also called adhesion. The mathematical formula of adhesion is described as follows:

$$F_\varphi = F_z \cdot \mu, \tag{9}$$

where F_φ is the ultimate adhesion between the wheel and the ground; F_z is the vertical load of the wheel.

In order to prevent the relative slip movement between the wheel and the ground, the vector sum of the driving torque provided by the motor for the wheel and the lateral force on the tire should be less than the limit adhesion force between the wheel and the ground.

$$|F_\mu| \le |F_\varphi| - |F_y|, \tag{10}$$

where F_μ is the wheel ground utilization force; F_y is the wheel lateral force.

When the driving force on the wheel exceeds the adhesion limit, the wheel will be in a slip state. When the vehicle is running normally, it is necessary to consider the ability of the wheel of the DDEV to resist external interference. The tire is required to have sufficient reserve adhesion while meeting the vehicle longitudinal driving and yaw torque requirements.

From the theoretical knowledge of ASB control strategy [23], on dry road conditions, the relationship between the longitudinal/lateral adhesion coefficient of the slip rate as shown in Figure 6. The optimal longitudinal slip rate value $\lambda_{opt\_log} = 0.18$ & adhesion coefficient $\mu_{opt\_log} = 0.85$ is

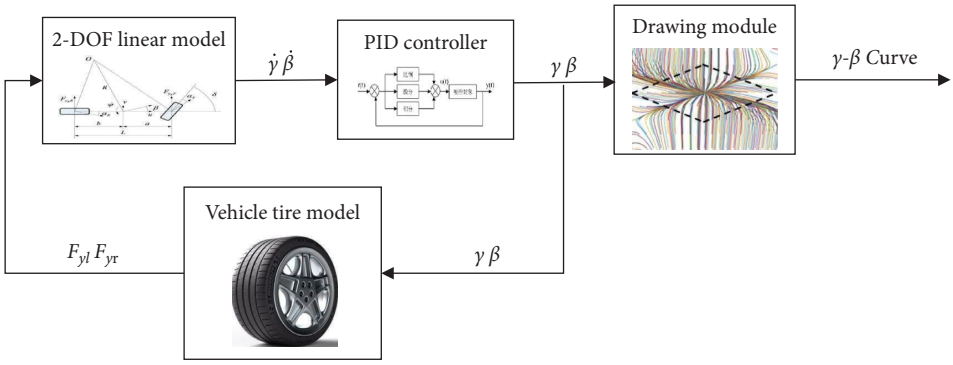

Figure 4: Simulation flow chart in β-γ.

Table 3: Stability boundary parameters with high adhesion coefficient at different speeds.

	v	$\lvert X\rvert$	$\lvert Y\rvert$
	30 km/h	0.22 rad	0.95 rad/s
$\mu = 0.8$	60 km/h	0.19 rad	0.83 rad/s
	90 km/h	0.13 rad	0.65 rad/s

Table 4: Stability boundary parameters with high speed at different adhesion coefficient.

	μ	$\lvert X\rvert$	$\lvert Y\rvert$
	0.8	0.125 rad	0.63 rad/s
$v = 90$ km/h	0.5	0.085 rad	0.48 rad/s
	0.2	0.029 rad	0.22 rad/s

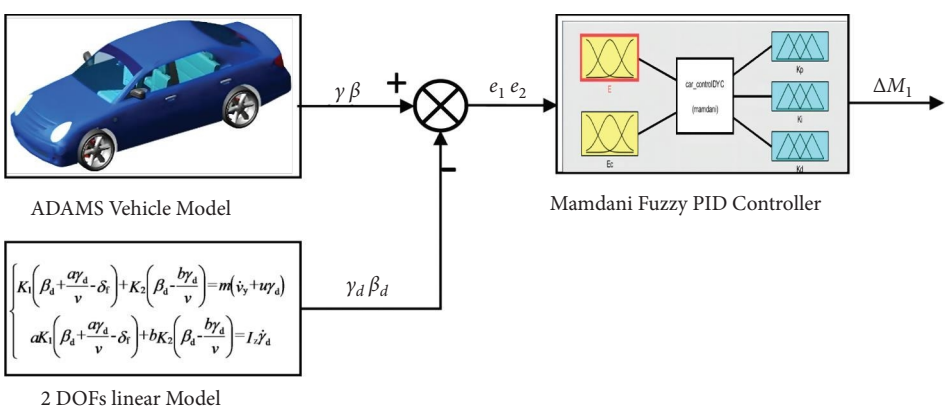

Figure 5: Structure diagram of DYC.

Table 5: Fuzzy controller rules.

$\Delta k_p/\Delta k_i/\Delta k_d$		e_c						
		NB	NM	NS	ZO	PS	PM	PB
	NB	PB/NB/PS	PB/NB/NS	PM/NM/NB	PM/NM/NB	PS/NS/NB	ZO/ZO/NM	ZO/ZO/PS
	NM	PB/NB/PS	PB/NB/NS	PM/NM/NB	PS/NS/NM	PS/NS/NM	ZO/ZO/NS	NS/ZO/ZO
	NS	PM/NB/ZO	PM/NM/NS	PM/NS/NM	PS/NS/NM	ZO/ZO/NS	NS/PS/NS	NS/PS/ZO
e	ZO	PM/NM/ZO	PM/NM/NS	PS/NS/NS	ZO/ZO/NS	NS/PS/NS	NM/PM/NS	NM/PB/ZO
	PS	PS/NM/ZO	PS/NS/ZO	ZO/ZO/ZO	NS/PS/ZO	NS/PS/ZO	NM/PM/ZO	NM/PB/ZO
	PM	PS/ZO/PB	ZO/ZO/NS	NS/PS/PS	NM/PS/PS	NS/PS/PS	NM/PB/PS	NM/PB/PB
	PB	ZO/ZO/PB	ZO/ZO/PM	NM/PS/PM	NM/PM/PM	NM/PM/PM	NB/PB/PS	NB/PB/PB

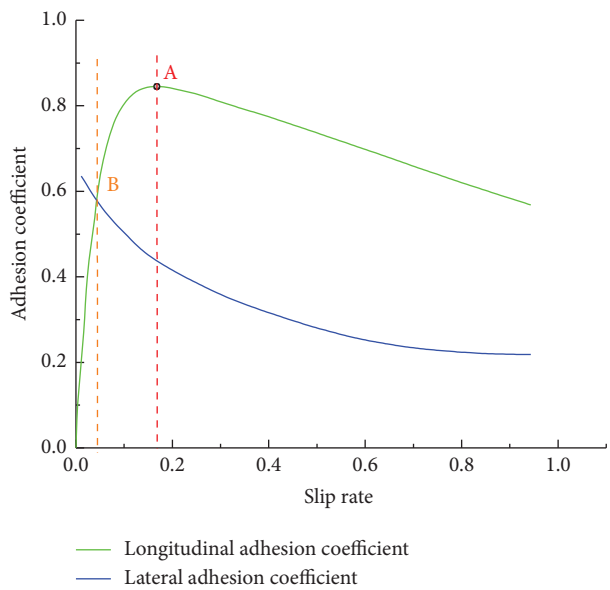

Figure 6: Curve of slip rate and adhesion coefficient.

obtained based on the adhesion coefficient curve of slip rate [11] which is located and selected at point A. Similarly, the optimal lateral slip rate value $\lambda_{opt\_lat} = 0.05$ & adhesion coefficient $\mu_{opt\_lat} = 0.6$ is obtained based on the adhesion coefficient curve of slip rate which is located and selected at point B.

The actual slip rate λ, which reflects the actual state of the vehicle is obtained by ADAMS/Car model. w_{rl}, w_{rr} and v_{rl}, v_{rr} according to the slip rate formula relate and expressed as follows:

$$\begin{cases} \lambda_{rl} = \dfrac{w_{rl} \times r - v_{rl}}{w_{rr} \times r} \times 100\%, \\ \lambda_{rr} = \dfrac{w_{rr} \times r - v_{rr}}{w_{rr} \times r} \times 100\%, \end{cases} \tag{11}$$

where λ_{rl}, λ_{rr} are the actual slip rate of the left and right rear wheels, respectively.

The difference $e_3 = \lambda - \lambda_{opt}$ is transmitted to the slip rate PID controller output ΔM_2 as shown in Figure 7.

From this we can see that,

$$\Delta M_2 = k_2 \times fpid(e_3), \tag{12}$$

where k_2 is the experience value, $fpid(e_3)$ is the PID controller.

Considering the longitudinal and lateral acceleration of the vehicle during acceleration and steering, the vertical load of left and right wheels are obtained as follows:

$$\begin{cases} F_{zrl} = \dfrac{mga}{2(a+b)} + \dfrac{mha_x}{2(a+b)} - \dfrac{mha_y}{2T_r} \\ F_{zrr} = \dfrac{mga}{2(a+b)} + \dfrac{mha_x}{2(a+b)} + \dfrac{mha_y}{2T_r} \end{cases}, \tag{13}$$

where F_{zrl} is the vertical load of the left rear wheel; F_{zrr} is the vertical load of the right rear wheel; g is the acceleration of gravity; a_x is the longitudinal acceleration; a_y is the lateral acceleration.

When the vehicle is steering, the load transfer will occur and the limit adhesion of the inner wheel will decrease while that of the outer wheel will increase. Therefore, in order to prevent the inner wheel from slipping, the driving torque of the inner wheel should be limited.

$$\frac{T}{r} + F_y \le F_{zr} \times \mu, \tag{14}$$

If the above-given formula is satisfied, then:

$$\begin{cases} T_{dl} = T_d, T_{dr} = T_d & \Delta M_2 = 0 \\ T_{dl} = T_d - \Delta T/2, T_{dr} = T_d + \Delta T/2 & \Delta M_2 > 0 \\ T_{dl} = T_d + \Delta T/2, T_{dr} = T_d - \Delta T/2 & \Delta M_2 < 0 \end{cases} \tag{15}$$

If not, then:

$$T = \left(F_{zr} \times \mu - F_y\right) \times r, \tag{16}$$

3.4. Modeling of DMSC. In order to better realize the demand of handling and stability control in the driving process of DDEV, the DMSC strategy based on DYC and ASR is proposed in this section.

3.4.1. Designing of DMSC. A single control cannot adapt to all working conditions of a vehicle. According to the evaluation index of vehicle handling and stability established by academician [9] and the characteristics of the two control modes, the slip rate is taken as the reference characteristic quantity for switching between the two control modes.

We can set the test and simulation conditions as shown in Figure 8 to confirm the characteristic slip rate threshold when the two control modes are switched.

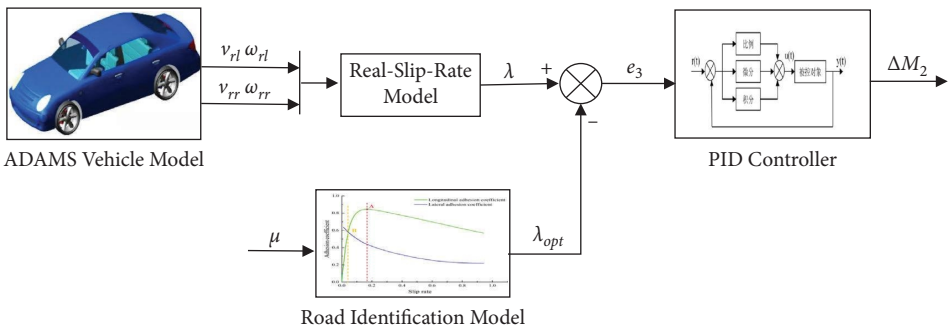

Figure 7: Structure diagram of ASR.

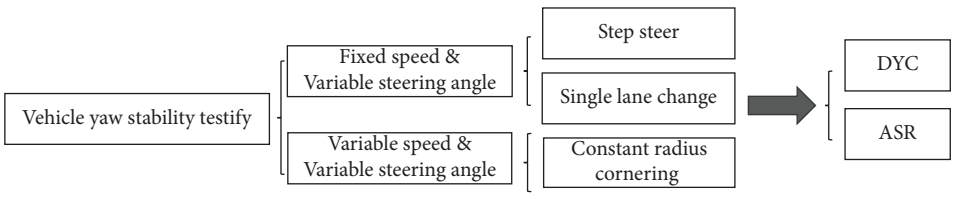

Figure 8: Classifications of test conditions.

After the simulation test conditions are set, the difference of yaw rate $REME(\gamma)$ is used as the evaluation index γ_i and $\gamma_{d,i}$. The deviation degree of the curve can reflect the difference of the control effect better.

$$REME(\gamma) = \sqrt{\frac{\sum_{i=1}^{n}\left(\gamma_i - \gamma_{d,i}\right)^2}{n}}. \tag{17}$$

The simulation parameters in Table 6 are set for DYC.

Two curves are obtained by simulation taking $REME(\gamma)$ as ordinate, w_r as the sum of curves in abscissa and λ as ordinate while w_r is the abscissa curve.

In Figure 9, the curve under the step steer test condition is analyzed when λ is above 0.15, $REME(\gamma)$ is small and the DYC effect at this stage is better. The curve analysis under single lane changes the test condition when λ is above 0.15 and the corresponding $REME(\gamma)$ curve is smaller which shows that the DYC effect is significant in this stage. Under the constant radius cornering test condition, the $REME(\gamma)$ curve is obviously small with w_r and when λ is between 0.15 and 0.4, the $REME(\gamma)$ curve suddenly changes from a larger value to a smaller value. The analysis shows that the DYC has more advantages when λ is between 0.15 and 0.4.

The simulation parameters in Table 7 are set for ASR.

Two curves are obtained by simulation and by taking $REME(\gamma)$ as ordinate, w_r as the sum of curves in abscissa, λ as ordinate and w_r as the abscissa curve.

In Figure 10, it can be seen from the curve under the step steer test condition that λ increases with w_r when λ is higher than 0.4. The control effect is better when λ is above 0.4. Analyzing the curve of the single lane change test, it can be concluded that the corresponding $REME(\gamma)$ curve is smaller than other stages when λ is above 0.4 which indicates that the ASR effect is more significant in this stage. Under the constant radius cornering test condition, the corresponding $REME(\gamma)$ curve is obviously smaller than other stages with w_r when λ is above 0.4 the $REME(\gamma)$ curve changes greatly at this stage. It can be seen that the effect of ASR has been shown. In conclusion, when λ is between 0.4 and 1 the $REME(\gamma)$ curve tends to decline or is in a low range which indicates that the ASR effect is superior.

Table 6: Simulation test parameters of DYC.

Test schemes	Parameters	Value and units
Step steer	v	60, 80, 100 km/h
	θ_c	0.5π rad
	μ	0.8
Single lane change	v	80, 90, 100 km/h
	θ_c	0.5π rad
	μ	0.8
Constant radius cornering	R	20, 30, 40 m
	$\dot{a}_y$	0.1 m/s^2/s

Combining with the simulation curve analysis in Figures 8 and 9. When λ is between [0.15 0.4], the effect of the DYC strategy is better. When λ is between [0.4 1], the effect of the ASR strategy is better. With DYC, the cosimulation strategy can better regulate the body posture. With ASR, it can better suppress wheel slip and vehicle loss of control. With DMSC, while correcting the body posture, it can also restrain the wheels from slipping, improve the handling stability of the vehicle on low-adhesion roads, and effectively prevent the vehicle from slipping out of control.

3.4.2. Judging of Switch. In order to prevent the frequent change of λ which is caused by complex road surface that eventually lead to misjudgment of vehicle ASR and DYC system. λ is used as the evaluation reference when $0.15 \le \lambda \le 0.4$, DYC is switched to apply torque to reduce λ. When $0.4 \le \lambda \le 1$, ASR is switched to control λ_{opt}.

Mode switching means that after switching the control system, the torque command of the drive motor is output

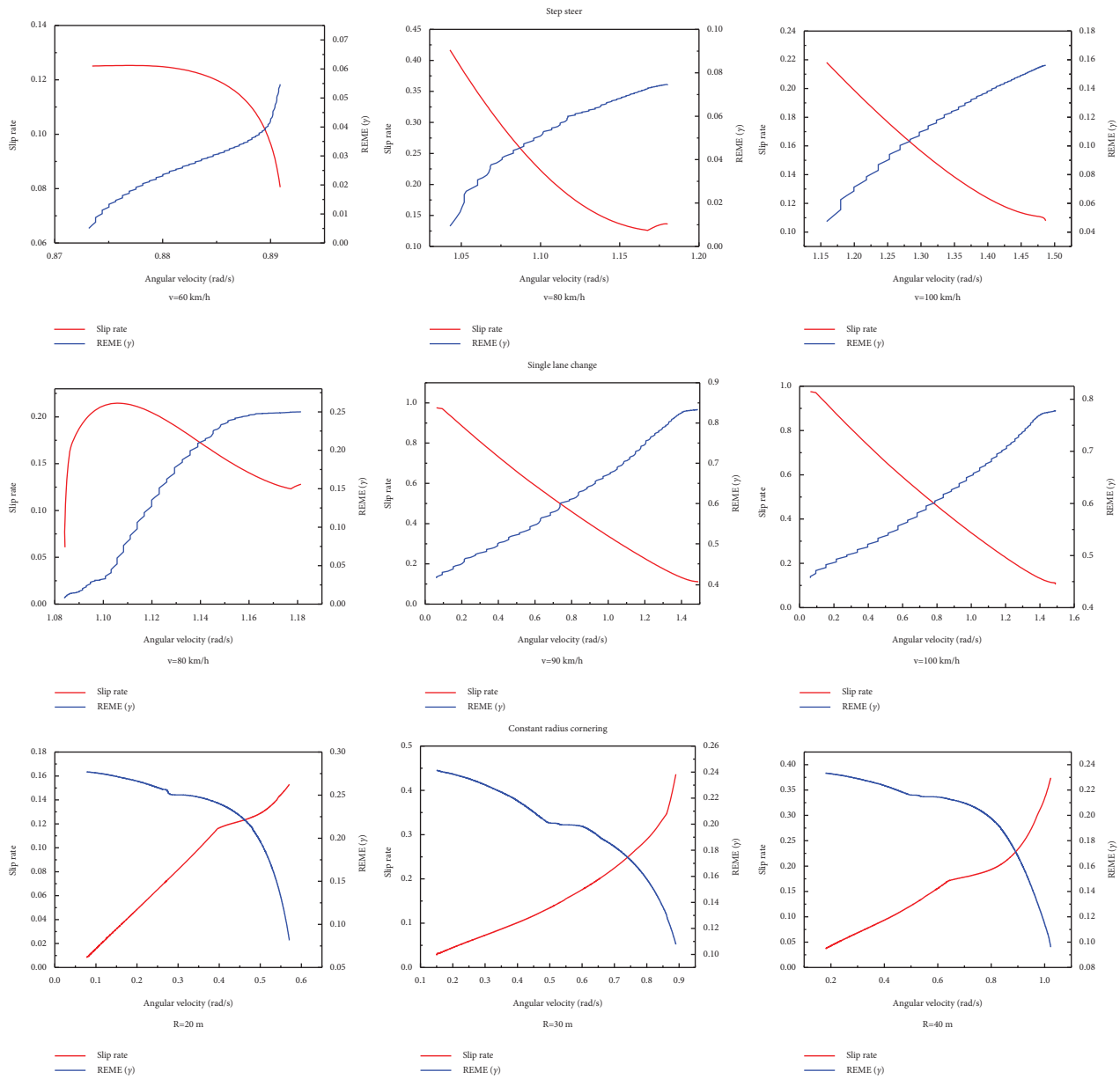

Figure 9: Simulation curve of DYC.

Table 7: Simulation test parameters of ASR.

Test schemes	Parameters	Value and units
Step steer	v	30, 40, 50 km/h
	θ_c	0.5π rad
	μ	0.3
Single lane change	v	40, 50, 60 km/h
	θ_c	0.5π rad
	μ	0.3
Constant radius cornering	R	20, 30, 40 m
	$\dot{a}_y$	0.2 m/s^2/s

by the corresponding control module. When the control mode is exited, the torque command of the drive motor is not directly output through the control module. The switching process is designed as flag = 0 and flag = 1, which is shown in Figure 11. In order to avoid oscillation during the model switching, to add the coordination gap between the DMSC change, but the gap value need to be validated and optimized by a real car.

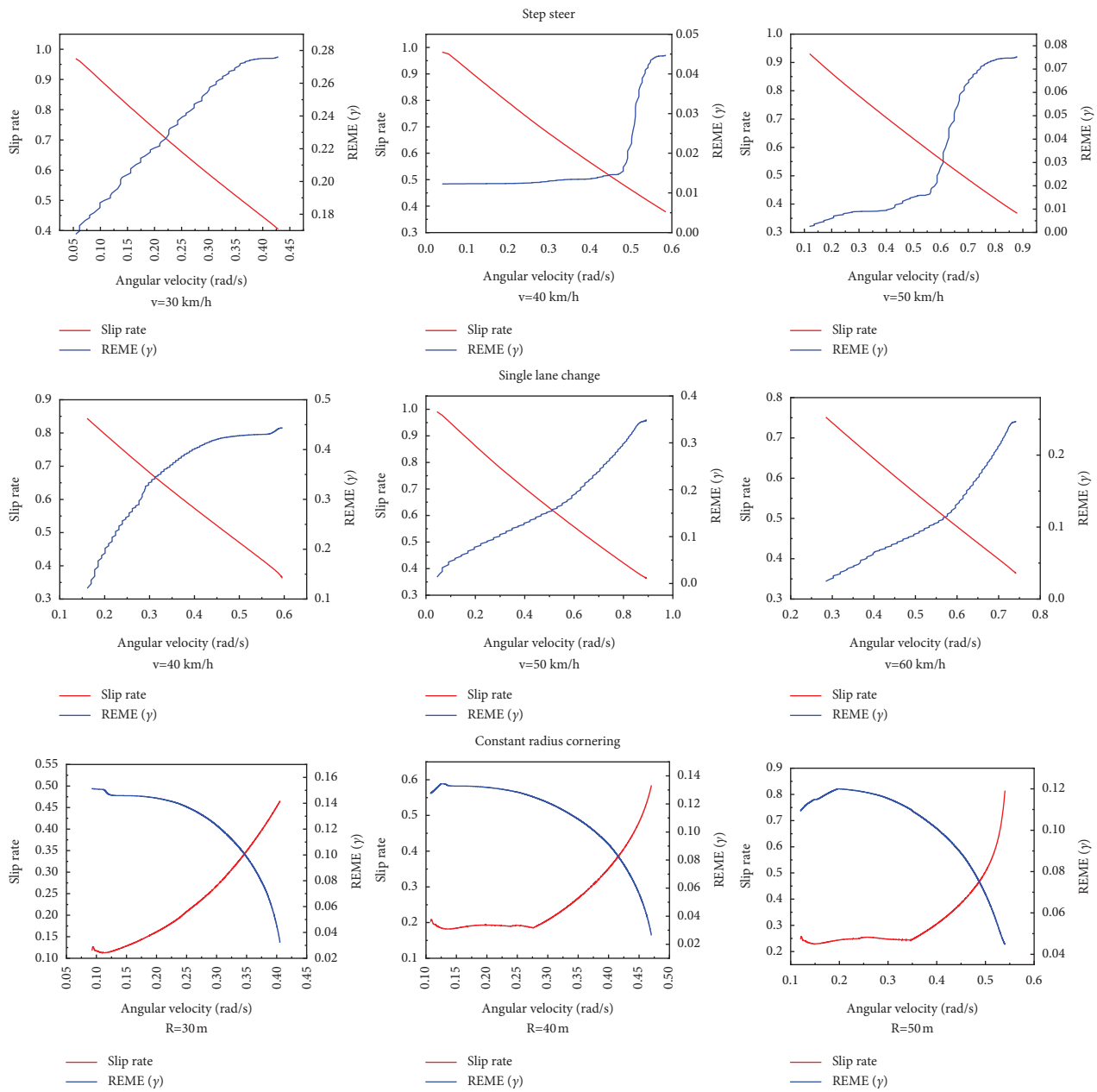

Figure 10: Simulation curve of ASR.

The control idea in Figure 11 is expressed in code as follows: (Algorithm 1)

Here, K is the pedal opening valve, θ_c is the steering wheel angle, and μ is the adhesion coefficient.

In this part, side slip angle and yaw rate are used as reference variables to study vehicle stability. When driving at high speed or on low-adhesion roads, the vehicle is easily unstable, and the center of mass slip angle can reflect the stable state of the vehicle. The yaw rate also increases gradually, which can better reflect the handling ability of the vehicle.

3.5. Vehicle Model. As shown in Figure 12, the actual yaw rate β and side slip angle γ parameters were obtained from ADAMS/Car model, β_d and γ_d were obtained from 2-DOF linear model, which is transferred to the fuzzy PID controller to obtain the correction torque ΔM_1. On the other hand, the actual linear speed of left and right wheels v_{rl}, v_{rr} and w_{rl}, w_{rr} are obtained by ADAMS/Car model, which are transmitted to the slip-rate PID control module to obtain the correction torque ΔM_2. The DYC or ASR torque value is obtained by the torque distribution module and transmitted to the mode switching module.

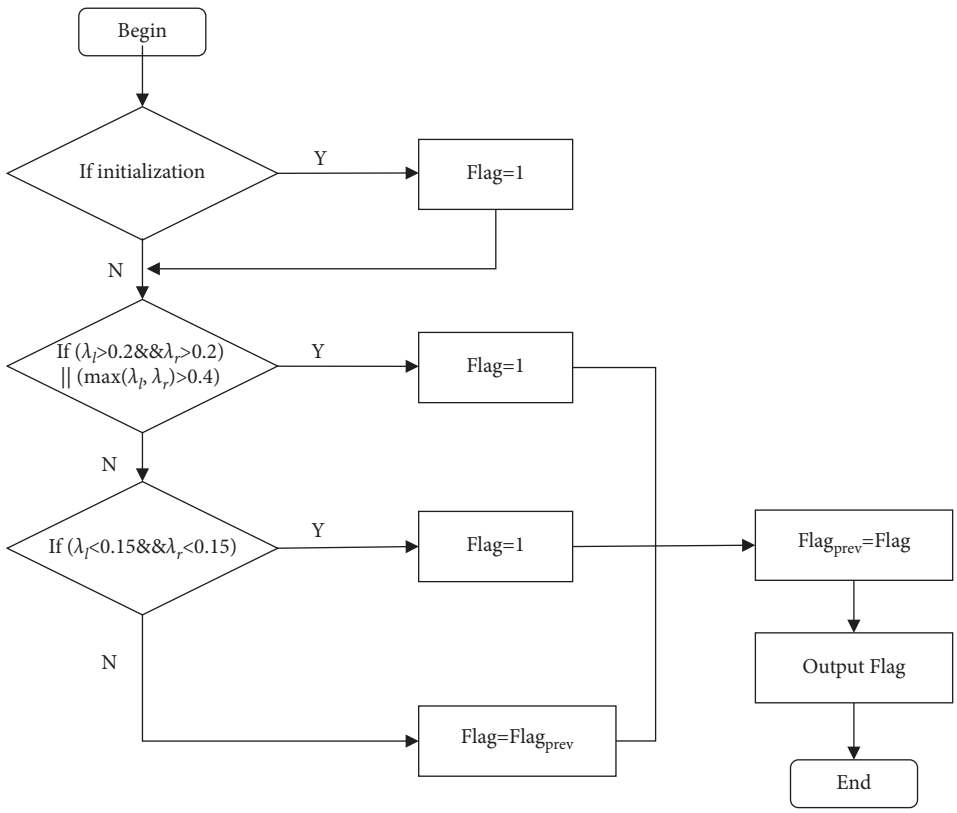

Figure 11: Flow chart of switching mode.

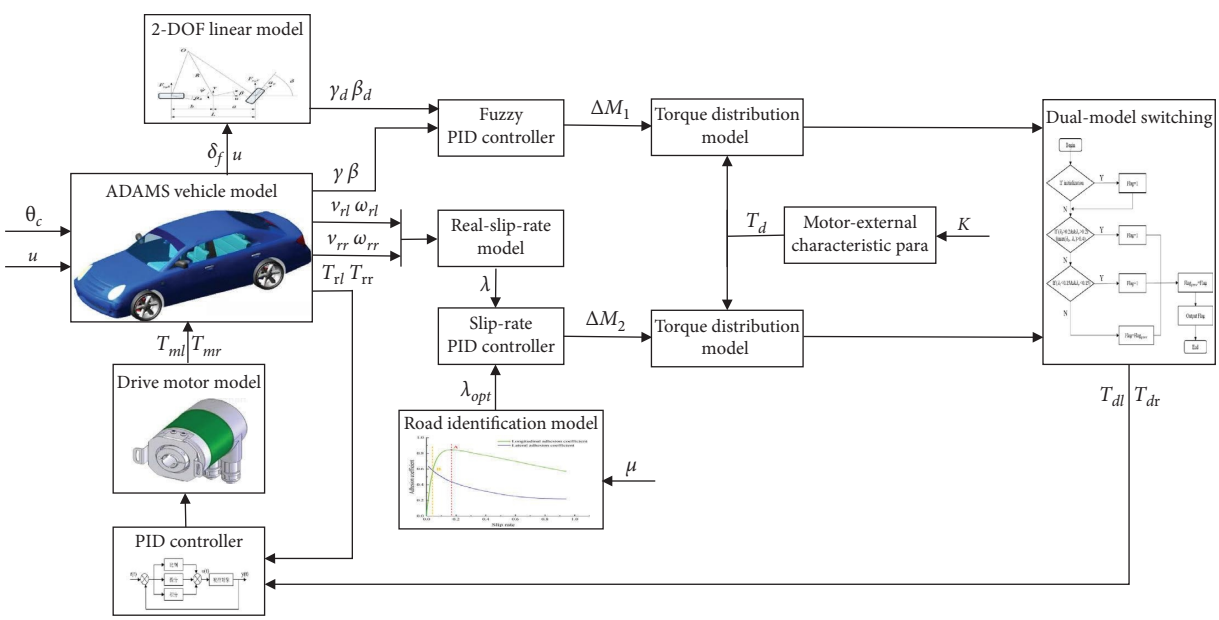

Figure 12: Vehicle control structure diagram.

T_{dl} and T_{dr} are obtained by ADAMS/Car model while T_{rl} and T_{rr} are input into the motor model established in the previous section. The outputs T_{ml} and T_{mr} act on the driving wheel to realize the control of vehicle handling and stability.

4. Validation and Analysis

The control strategy is validated under the cosimulation platform of the software ADAMS/Car and MATLAB/Simulink. The parameters regarding the vehicle and the

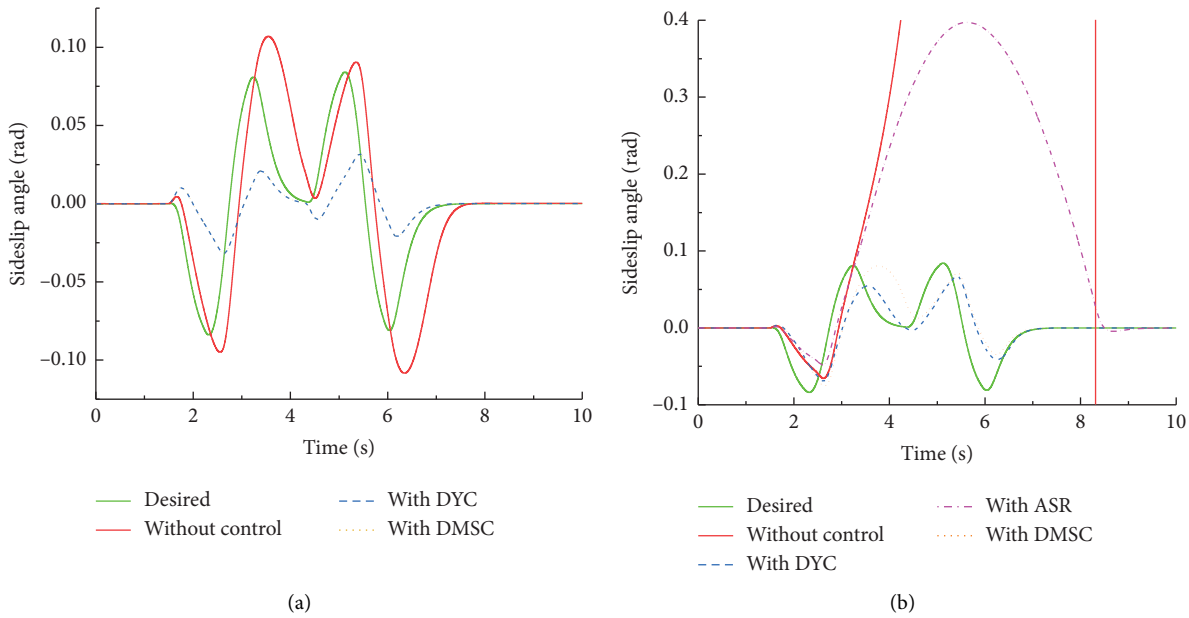

Figure 13: Sideslip angle. (a) Case 1 (b) case 2.

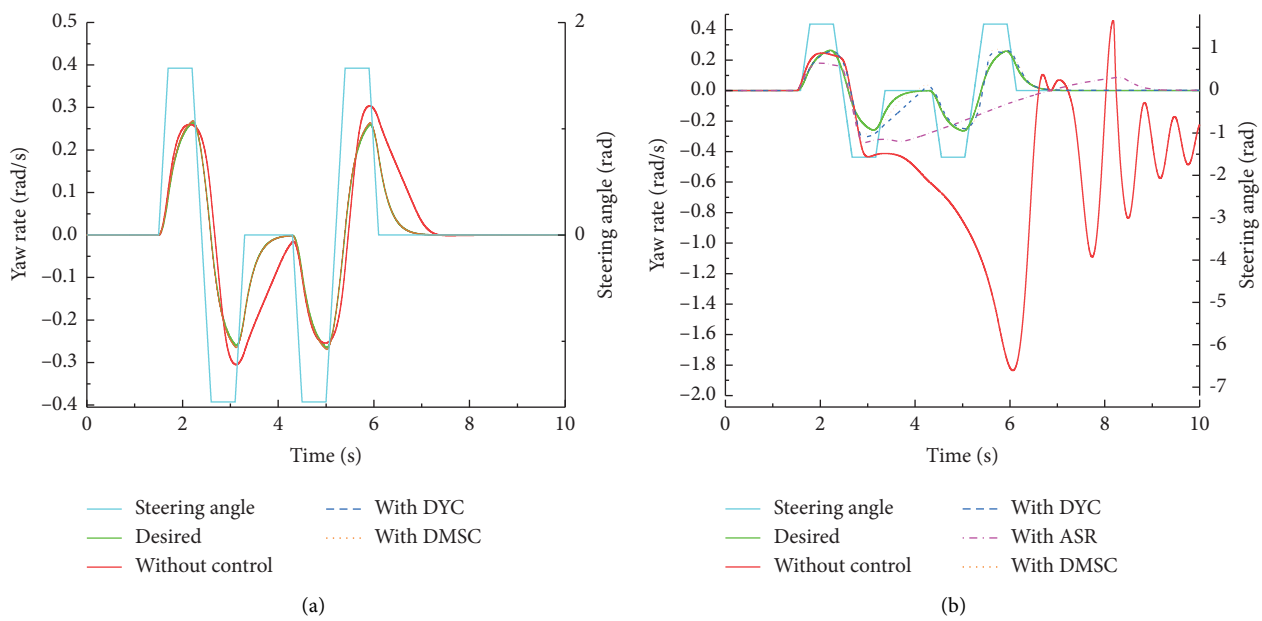

Figure 14: Yaw rate. (a) Case 1 (b) Case 2.

controller are illustrated in the above-given tables. In the following, the tests of Double lane-change is carried out to verify the effectiveness of the proposed strategy.

Case 1: 80 km/h, μ is 0.8, and θ_c is 0.5 πrad
Case 2: 60 km/h, μ is 0.3, and θ_c is 0.5 πrad

In the following, the validations are divided into two parts to illustrate the superiorities of the DMSC, namely, benefits in control reference and in DMSC and torque allocation.

Figures 13–16 depict the performance of four references under four modes, without control, with DYC, with ASR and with DMSC. Table 8 lists the two reference values under four modes.

Under case 1, the mode of "without control," which shows a worse handling experience and the tracking performance of the yaw rate is poor. Although there is no wheel slip, the trajectory deviation of the double line shift is large, the max absolute value of sideslip angle achieve 0.11. The mode of "with DYC" effect, the curve of yaw rate shows excellent tracking performance, the trajectory is smooth, it can better complete the Double lane-change action and return to the original lane, the wheels do not slip and the

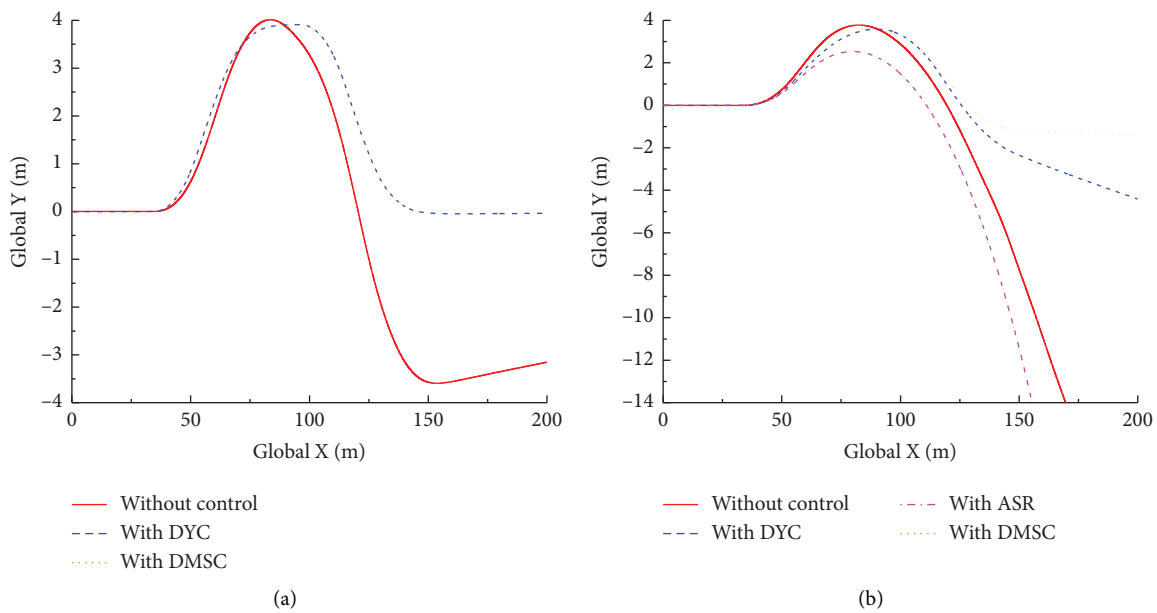

Figure 15: Path tracing. (a) Case 1 (b) case 2.

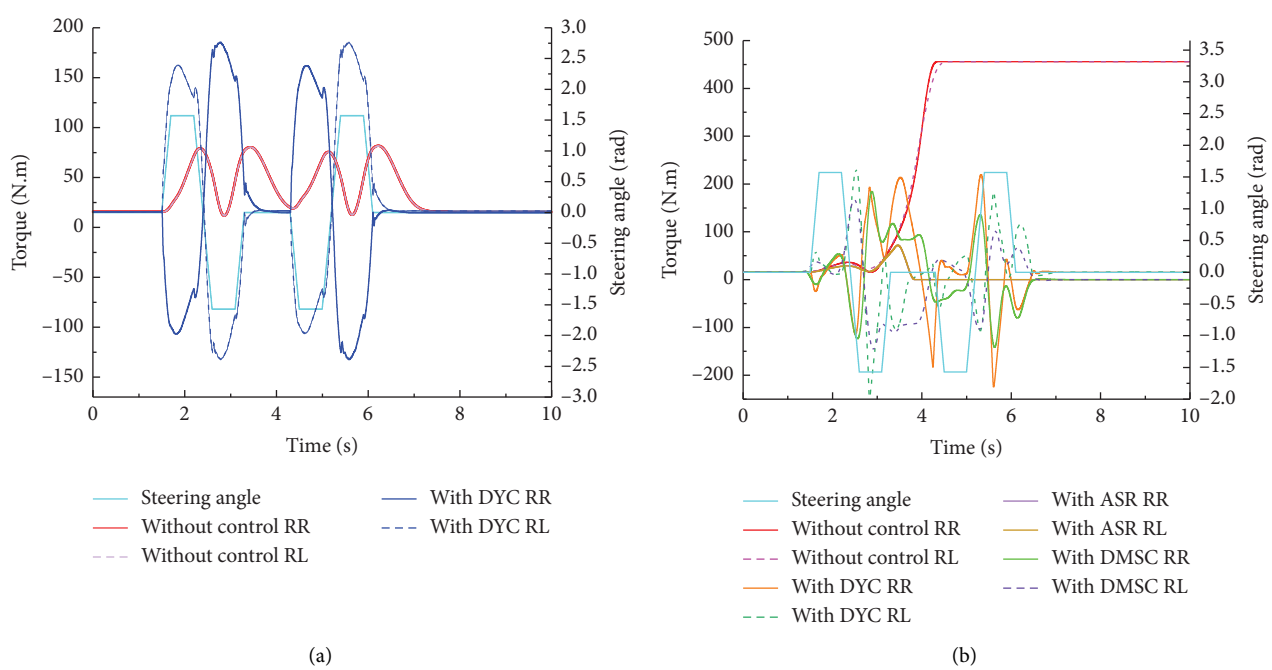

Figure 16: Torque. (a) Case 1 (b) Case 2.

vehicle speed fluctuates slightly. Since case1's μ is 0.8, ASR has no intervention control, the results of DYC only and DMSC are completely consistent.

Case 2 depicts four modes, without control, with DYC, with ASR and with DMSC. Completely, the mode of "without control" is out of control, the yaw rate curve can not be tracked, the wheels completely slip, the vehicle speed fluctuates greatly, and the body is in an unstable state.

With DYC shows a certain control effect, the vehicle can be stabilized in the end, but there is an obvious slippage trend. The yaw rate value is acceptable, but it is offset due to slippage and completely the trajectory is impossible to return original exercise direction. The mode of "with ASR" is able to control the body to a stable state, but completely unable to follow the sideslip angle and complete the Double lane-change movement. Under DMSC, the yaw rate curve follows better, the wheel slip

```
If (λrl > 0.2&& λrr > 0.2)||(max(λrl, λrr) > 0.4)
{
   DYC2ASR_Flag = 1;
}
else
{
   //do nothing
}
If (λrl < 0.15&& λrr < 0.15)
{
   DYC2ASR_Flag = 0;
}
else
{
   //do nothing
}
```

Algorithm 1: The code of switching mode.

Table 8: Comparison of two reference values under four modes.

Test case	Control model	Max|Yaw rate| (rad/s)	Max|Sideslip angle| (rad)
Case1	Desired	0.26	0.08
	Without control	0.305	0.11
	With DYC	0.258	0.03
	With DMSC	0.258	0.03
Case2	Desired	0.26	0.08
	Without control	1.83	\
	With DYC	0.26	0.055
	With ASR	0.176	0.39
	With DMSC	0.26	0.075

rate is controlled after ASR is involved, and the speed of the vehicle drops slightly after ASR is involved, and the trajectory performance is better, it can return to the driving direction greatly.

5. Conclusion

The control effects of DYC and ASR on handling and stability performance are presented based on the DDEV model in this study. Firstly, the subsystem model of each vehicle part is established using the ADAMS/Car software while the vehicle dynamic model and electric power flow model are established based on MATLAB/Simulink software, and the two softwares combine the cosimulation platform. Then, the phase trajectory stability domain, DYC model, the ASR model and DMSC model are designed and built based on the cosimulation platform. Just to simulate and verify the DMSC. Finally, the simulation curves show that the DMSC can effectively prevent DDEV from entering the dangerous limit driving state when turning and driving. The strategy has a more significant control effect needed to meet the requirements [26] of the driving safety of the vehicle and handling stability [27].

Data Availability

The datasets used and analyzed during the current study are available from the corresponding author on reasonable request. The paper has been presented as PREPRINT in Research Square according to the following link: https://www.researchsquare.com/article/rs-604895/v1.

Conflicts of Interest

The authors declare that there are no conflicts of interest.

Acknowledgments

This work was supported in the part by the Natural Science Foundation of Zhejiang Province under grant under Grant no. LY21E050001 and by the Open Research Fund of Anhui Engineering Technology Research Center of Automotive New Technique, under Grant no. QCKJ202105.

References

[1] assets.researchsquare, “Integra ted DYC and ASR Mixed Control of Distributed Drive Electric Vehicle Using CoSimulation Methodology" in 2021 Based on the below Link,”

2021, https://assets.researchsquare.com/files/rs-604895/v1_covered.pdf?c=1631870833.

[2] K. Juyong, C. Wanki, and Y. Jinho, "Driving control algorithm for maneuverability and lateral stability for application to 4WD series hybrid vehicle," *IFAC Proceedings Volumes*, vol. 43, no. 7, pp. 168–173, 2010.

[3] L. Xiong, X. Gao, and T. Zou, "Electro hydraulic hybrid distribution stability control of distributed drive electric vehicles," *Journal of Tongji University*, vol. 44, no. 6, pp. 922–929, 2016.

[4] Z. Junjun, W. Zhenpo, and Z. Lei, "Braking/steering coordination control for in-wheel motor drive electric vehicles based on nonlinear model predictive control," *Mechanism and Machine Theory*, vol. 142, 2019.

[5] L. JingXing, Z. WeiChao, and Z. Hong, "Integrated energy-oriented lateral stability control of a four-wheel-independent-drive electric vehicle," *Science China Technological Sciences*, vol. 62, no. 12, pp. 2170–2183, 2019.

[6] E. Esmailzadeh, A. Goodarzi, and G. R. Vossoughi, "Optimal yaw moment control law for improved vehicle handling," *Mechatronics*, vol. 13, no. 7, pp. 659–675, 2003.

[7] S. Yu, C. Wuwei, and C. Liqing, "Joint simulation of vehicle stability control based on and MATLAB," *Journal of Mechanical Engineering*, vol. 47, no. 16, pp. 86–92, 2011.

[8] H. Taghavifar, C. Hu, L. Taghavifar, and Qin, "Optimal robust control of vehicle lateral stability using damped least-square backpropagation training of neural networks," *Neurocomputing*, vol. 384, pp. 256–267, 2020.

[9] Y. Youn and S. Song, "Improvement of vehicle directional stability in cornering based on yaw moment control," *KSME International Journal*, vol. 14, no. 8, pp. 836–844, 2000.

[10] D. Ronghua, M. Siyu, and H. Lin, "Simulation of torque distribution control strategy for hybrid braking system of distributed drive electric vehicle," *Automotive Engineering*, vol. 41, no. 3, pp. 327–333+345, 2019.

[11] Z. Fengjun, *Research on Integrated Control Strategy of Distributed Drive Electric Vehicle Based on Double Layer Architecture*, Beijing University of technology, Beijing, China, 2014.

[12] W. Zhifu, Y. Zhou, and L. Guangzhao, "The sliding mode control about ASR of vehicle with four independently driven in-wheel motors based on the exponent approach law," *Energy Procedia*, vol. 88, pp. 827–832, 2016.

[13] H. Hongwen, P. Jiankun, and X. Rui, "An acceleration slip regulation strategy for four-wheel drive electric vehicles," *Based on Sliding Mode Control*, vol. 7, no. 6, pp. 3748–3763, 2014.

[14] Y. Guodong, W. Shanbao, and J. Xianjian, "Optimal Slip Ratio Based Fuzzy Control of Acceleration Slip Regulation for Four-Wheel Independent Driving Electric Vehicles," *Mathematical Problems in Engineering*, vol. 2013, Article ID 410864, , 2013.

[15] D. Xiaolin, Z. Lei, and W. Zhenpo, "Acceleration slip regulation for four-wheel-independently-actuated electric vehicles based on road identification through the fuzzy logic," *IFAC-PapersOnLine*, vol. 51, no. 31, 2018.

[16] K. Hiroaki, S. Hideo, and S. Ichiro, "Optimal slip ratio estimator for traction control system of electric vehicle based on fuzzy inference," *Electrical Engineering in Japan*, vol. 135, no. 3, pp. 56–63, 2001.

[17] L. Fajun, W. Yajun, and D. Yali, "Simulation Research of Fuzzy Logic Control for ASR Based on MATLAB," *Ship Electronic Engineering*, vol. 11, 2011.

[18] H. Long, W. Wenge, and P. Jingyang, "Research on integrated control strategy of direct yaw moment and drive anti slip for electric vehicles," *Automotive technology*, vol. 2019, no. 6, pp. 41–46, Article ID 5170492, 2019.

[19] C. Wuwei, L. Xiutian, and W. Qidong, "Extension coordinated control of four wheel independent drive electric vehicles by AFS and DYC," *Control Engineering Practice*, vol. 101, no. C, 2020.

[20] L. Daoyuan, H. Song, and W. Sen, "Direct yaw-moment control of electric vehicle with in-wheel motor drive system," *International Journal of Automotive Technology*, vol. 21, no. 4, 2020.

[21] Wang Tao Jiang Jinfeng Lin Youting Lin Qiufeng Zhang Wenming, "Driver model for obstacle avoidance based on CarSim," *Journal*, vol. 26, no. 5, 2010.

[22] H. B. Pacejka, "Nonlinearities in road vehicle dynamics," *Vehicle System Dynamics*, vol. 15, no. 5, pp. 237–254, 2007.

[23] Yu. Zhisheng, "ElementaryVehicleDynamics," *China Machinery Press*, vol. 03, 2009.

[24] S. Inagaki, I. Kushiro, and M. Yamamoto, "Analysis on vehicle stability in critical cornering using phase-plane method," *JSAE Review*, vol. 16, no. 2, p. 187, 1995.

[25] K. Koibuchi, M. Yamamoto, and Y. Fukada, "Vehicle Stability Control in Limit Cornering by Active Brake," *SAE International Congress & Exposition. Detroit*, Article ID 960487, 1996.

[26] G. Jinghua, L. Ugong, and L. Keqiang, "Coordinated path-following and direct yaw-moment control of autonomous electric vehicles with sideslip angle estimation," *Mechanical Systems and Signal Processing*, vol. 105, pp. 183–199, 2018.

[27] P. Xiaofei, L. zhaodu, and M. Guocheng, "Multi-mode switching control of automobile adaptive cruise system," *Journal of Mechanical Engineering*, vol. 48, no. 10, pp. 96–102, 2012.